SCIENTIFIC Publishing Limited

New Energy Exploitation and Application
http://ojs.ukscip.com/index.php/neea

Article

Transistor Cooling with Nanoparticle Enhanced Phase Change Material

Mohammad Yaghoub Abdollahzadeh Jamalabadi

Department of Engineering, Faculty of Marine Engineering, Chabahar Maritime University, Chabahar 99717-56499, Iran

* Correspondence: my.abdollahzadeh@cmu.ac.ir

Received: 4 December 2024; **Revised:** 13 December 2024; **Accepted:** 17 December 2024; **Published:** 18 December 2024

Abstract: In the current paper, the cooling of a bipolar transistor with phase change is investigated. The nanoparticle-enhanced phase change material (NEPCM) can transform from a solid to a liquid by absorbing and releasing energy. The NEPCM is composed of various nanoparticles such as silver, Copper, Aluminum Oxide, Copper (II) oxide, Titanium dioxide, graphene nanoplates, single and multi wall carbon nano tubes (SWCNT- MWCNT) suspended in normal TH29 phase change material. The synthesized NEPCM suspension is used as a passive cooling control system. Heat is uniformly distributed in the sidewall of the heat sink. As sensing and latent heat are absorbed from the transistor walls, the working fluid flows through the storage while because of natural convection inside the storage the Rayleigh–Bénard convection cells created and enhanced the heat transfer management. The volume fraction of added particles, heating power, and strength of streamline affect the controlling parameters of the system such as heat transfer rate, maximum allowable temperature, and thermal performance. The time of process regarding conducted numerical experiments to evaluate the solid-liquid interface through various particles are MWCNT, GNP, SWCNT, Al_2O_3, TiO_2, CuO, Cu, and Ag respectively. Through the various materials, the maximum temperature on the transistor surface is obtained by SWCNT, GNP, MWCNT, Ag, Cu, Al_2O_3, CuO, and TiO_2, respectively. The results presented here and conducting a complete investigation of heat sink storages can be used in transistors or various electronic cooling with the aid of nanofluids.

Keywords: Transistor; Cooling; Thermal Performance; Nanoparticle; Passive Control

1. Introduction

Electronics cooling system is an impressive engineering application that deals with the optimal working condition of electronic parts under heat generated. As thermal challenges become more complex, engineers utilize state-of-the-art simulation and measurement tools. In passive cooling, components are cooled by conduction, convection, and radiation from the environment. An enclosure used for power electronics generates massive waste heat due to the presence of high-power electronic components. Phase Change Material (PCM) is a material that have higher thermal capacity rather than normal materials. If the cabinet's internal temperature was rising above acceptable levels, posing a risk of equipment failure in the event of overheating. One of the technologies for controlling thermal management of electronic parts is the use of thermal storage materials.

By changing their physical state PCM can store thermal energy. It is necessary to have a significant difference between daytime and nighttime temperatures for the phase change to occur. Effects of Brownian motion [1] and change of thermophysical properties [2] are studied before. The enhanced thermophysical properties of freezing Nano-particle Enhanced Phase Change Material (NEPCM) make it a good candidate to cool bipolar transistors.

Electric heating occurs in every system where electric current is conducted and the material has finite conductivity. The unwanted by-product of current conduction is electric heating, also known as Joule heating. A transistor and copper pathway are simulated as part of this circuit board model. By simulating the transistor, we can estimate its operating temperature. In this simulation, a heat sink mounts the power transistor. As a result, researchers investigate whether the designed thermal storage is better than the condition that system works without heat sinks [3].

PCMs are made from organic materials containing long chain molecules, primarily carbon and hydrogen. Most of them change phases above zero degrees centigrade and exhibit high orders of crystallization when frozen. NEPCM is used for control of a subcooled flow boiling [4], and cooling of surface wave resonator [5]. Ali [6] shows the efficiency of new NEPCM. Such materials help the cooling of photovoltaic systems [7]. PCM serves as a High-performance heat sinking [8] in a thermal management system from micro size [9–12] to macro size [13]. A cooling device in a power supply unit is usually included in enclosures (made of aluminum over printed circuit board) to prevent excessively hot temperatures from damaging electronic components. In a power supply unit, the internal component is cooled by using an extracting fan and perforated grille. The geometry Temperature and fluid velocity fields of an enclosure with fan and grille are plotted in Figure 1. A curve in Figure 1 representing fluid streamline inside the contours of static pressure difference is provided by fan inside a computer case.

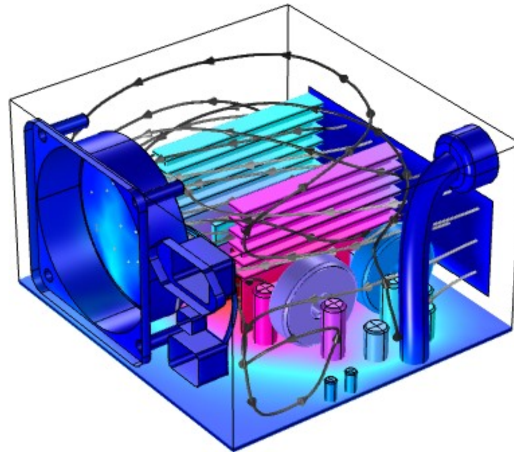

Figure 1. Temperature and fluid velocity fields of an enclosure with fan and grille.

The efficiency of using nanoparticles inside a low Reynolds numbers microchannel with ribs [14], at various microchannel height [15] was proved. In radios, computers and calculators, transistors are the building blocks of electronics. Heat transfer is a typical component of electrical systems; electric heating is an unwanted function of current conduction. A transistor containing copper pathways and a small part of a circuit board serves as the basis for this simulation. Calculation of effective fluid properties [16] as a function of temperature [17], to use in convective heat transfer of NEPCM [18] in various low Reynolds numbers microchannel heat sink [19] was performed in many studies [20]. The range of components' dissipated heat rates are Transistor cores 25 (W), transformer coil 3–5 (W), Inductors 2 (W), and capacitors 1–3 (W). The calculated sample of forced convection cooling of an enclosure with fan and grille as shown in Figure 1 expected the maximum 40 degrees of centigrade increase in temperature (at the middle of the circuit) and 1.5 m/s natural convection velocity for the air. Nusselt numbers could be improved by PCM layer embedded ceiling of a low Reynolds numbers microchannel [21] or used by various particle ratio [22] for best hydrothermal performance. A review on heat transfer enhancement by nanofluids [23, 24] shows the efficiency of NEPCMs. Due to undesirable electric heating, the transistor can operate at a temperature significantly higher than room temperature. Switching and amplifying electronic signals are performed with transistors. Depending on how they are packaged, transistors vary in size. Due to their more powerful power output, power transistors are larger. To prevent overheating and improve cooling, these packages can be attached to a heat sink.

The fabrication [25], characterization [26] as well as engineering applications in mini channel heat sink [27] are investigated experimentally [28, 29]. A recent review can be found in reference [30]. As illustrated in Figure 1 it

is often necessary to cool electronic systems, such as in hybrid cars, every system has its own acceptable operating temperature range. The maximum and minimum temperatures of semiconductors vary depending on the semi-conductor material proper- ties, the transistor type, and the design of the device, so one can reach temperatures between −55 °C and 125 °C.

The amount of stored thermal energy in latent heat systems and the time it takes to charge, and discharge are strongly affected by heat transfer modes that exist in the system. When NEPCMs are applied to an electronic system, they accelerate the charging and discharging process, but at the same time, they reduce the amount of energy stored [5]. As a common approach to solve the issue, nanoparticles can be dispersed in the common PCM to enhance thermophysical properties. The literature has indicated that the performance of storage systems can be negatively affected by the addition of nanomaterials above a certain concentration. It is therefore necessary to consider the properties and concentrations of nanomaterials. The aim of current study is to investigate the effect of differences in thermophysical properties on thermal cooling performance. There has been no research which used NEPCM in electronic cooling systems, especially those used in transistor applications. In the current paper, other than various NEPCM used to cooling of the power transistor, a multi-physics simulation was conducted to see the cooling effect of NEPCM while attached as a cavity to a transistor.

2. Mathematical Modelling

A representation of the mathematical problem is exhibited in Figure 2. Figure 2a plots the schematic of the transistor and current directions, Figure 2b plots the sampling transistor, and Figure 2c shows how the heat sink attaches to the transistor via the copper plate. As seen in Figure 2c, the model's geometry was used in the simulation. Through- hole mounting is used to mount power transistors on circuit boards. Copper routes and transistor pins on a transistor chip are connected by solder, which is inserted into the holes. The internal surface of a transistor chip is shown here as a thin structure, which can be considered very thin. Heat transfer is assumed to be negligible with the chip connected to the pins. Copper is used for the back part of the transistor package, which could be clamped to a heat sink. Its thermal properties match those of the transistor chip. 60Sn − 40Pb (60 tin and 40 lead) solder material is used to solder the copper pins. The circuit board is made of FR4. A glass-reinforced epoxy laminate material classified as FR-4 is a NEMA grade designation. Flame-resistant (self-extinguishing) fiberglass cloth with epoxy resin is the basis of FR-4, a composite material.

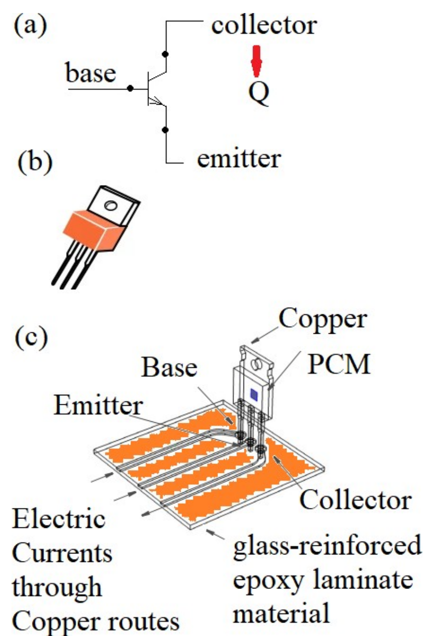

Figure 2. Key aspects of a transistor's configuration and integration in electronic systems (**a**) General symbolic configuration of the transistor and electric current directions; (**b**) sample transistor; (**c**) heat sink attaches to the transistor via the copper plate and transistor connections to the electronic board.

The solder, cables, and pins conduct current inside the electric circuit. Joule heating involves fully coupled heat transfer and heat production. Transistors only transfer and produce heat. The transistor chip produces some heat internally, and convection cooling takes place at all external boundaries with the environment (h = $W/(m^2K)$). Keeping the fan off will result in this value of heat transfer coefficient, which represents the worst-case scenario. Temperatures here are 20 °C. Current flows from the copper routes to the circuit board through the left vertical boundaries of the base, emitter, and collector routes. Electric connections are at the bottom.

2.1. Electric Currents

To model the Electric Currents in the system the Gau equation is used as Equation (1)

$$\nabla(-\sigma\nabla V + J_e) = Q_{j,v}, \tag{1}$$

Electric conductivity (σ) values are presented in Table 1.

Table 1. Electric conductivity.

Material	Electric Conductivity (S/m)
Cu	5.998×10^7
Solder (60Sn-40Pb)	6.67×10^6

Figure 2 displays each terminal and the voltage of base-emitter (VBE) where a constant voltage at collector-emitter (V_{CE} =0.5 Volts) is applied. the base current can be calculated from the other currents as following

$$IB = -IE - IC, \tag{2}$$

When the current is measured at the boundary of the route leading to the emitter, (I_E = 0.2A) with the Current density of collector and emitter routes which calculates by following equation

$$j_E = j_{CE}, \tag{3}$$

Which is equal to 100000 A/m2 and at the boundary of the route, there is a current (I_C = 0.1998A) which calculates by

$$j_C = (1 - 10^{-3})j_{CE}, \tag{4}$$

flowing to the collector at the boundary. A distinction in absolute current between the emitter and collector values corresponds to the current at the boundary of the route connecting the emitter to the collector (around 0.2 mA) which calculated by

$$j_B = 10^{-3} j_{CE}, \tag{5}$$

Figure 3 presents electric modeling schematic of a computational domain bipolar transistor in which the electric current is insert normally from three gates at the left and ground points as zero voltage given by

$$V = 0, \tag{6}$$

of each line are at the transistor.

2.2. Thermal Conduction in Solid

Equation of conservation of Energy in solid parts without heat generation is

$$\frac{\partial T}{\partial t} + \nabla \cdot (-\alpha \nabla T) = 0, \tag{7}$$

while in the electric parts keep at following modification

$$\frac{\partial T}{\partial t} + \nabla \cdot (-\alpha \nabla T) = \frac{Q}{\rho Cp}, \tag{8}$$

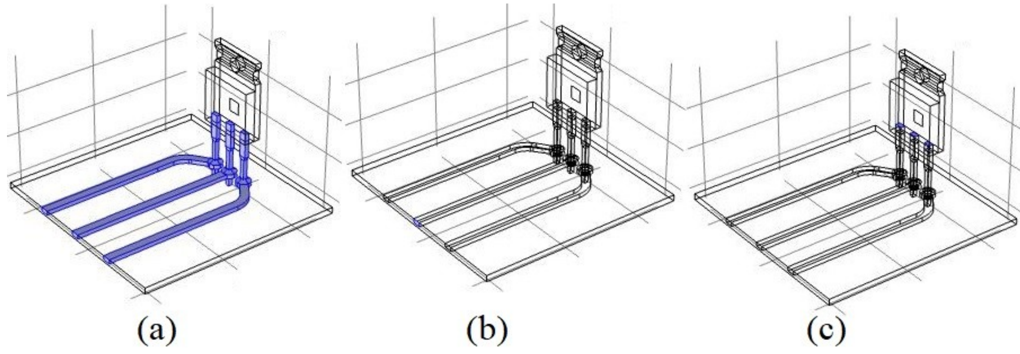

Figure 3. Electric modeling schematic: (**a**) Simplified cross-section through a bipolar transistor showing the electric structure of the device; (**b**) Circuit input shows the cross- section of input base electric current in an emitter configuration; (**c**) ground points of the electric computational domain inside the transistor.

is used and joule heating calculated by

$$Qe = -\nabla V \cdot J \tag{9}$$

As well, to consider heat transfer coefficient with the environment (T = 293.15[K]) constant value(5[w/mK]) is considered as the following equation

$$q" = 5(T - 293.15) \tag{10}$$

An adiabatic (zero gradient) is considered for the bottom of the board and symmetry planes of the system as boundary condition. Boundary heat source strength on the transistor square with a 3 mm length is considered as uniform given by

$$q = 105 \tag{11}$$

in SI units (W/m^2)

2.3. Heat and Fluid in NEPCM

The NEPCM fluid flow is laminar, incompressible, unsteady state, and Newtonian flow. It does not consider the dissipation of viscous fluid, the transfer of radiation heat, the expansion of PCM volumes, and the melting under close contact. Based on the assumptions of transient fluid analysis of the NEPCM the governing equations of fluid flow are considered as

The equation of conservation of Mass is as follow:

$$\partial_t (\rho) + \partial_x \left(\rho u_y\right) = 0, \tag{12}$$

with no-slip wall boundary condition. The equation of conservation of Momentum in x –direction is:

$$\rho \frac{\partial u}{\partial t} = \mu \nabla^2 (u) - \partial_x (p), \tag{13}$$

The equation of conservation of Momentum in y-direction is:

$$\rho \frac{\partial v}{\partial t} = \mu \nabla^2 (v) - \partial_y (p), \tag{14}$$

The equation of conservation of Momentum in z –direction is:

$$\rho \frac{\partial w}{\partial t} = \mu \nabla^2 (w) - \partial_z (p) - \rho g \beta (T - T_{ref}), \tag{15}$$

Finally, the conservation of Energy is governed by following equation:

$$\rho \frac{\partial H}{\partial t} + \nabla \cdot (-k \nabla T) = 0, \tag{16}$$

Enthalpy becomes summation of Sensible heat and latent heat term

$$H = C_p \int dT + \begin{cases} 0, T < T_{sld} \\ L, T \geq T_{lqd} \\ \frac{T - T_{sld}}{T_{lqd} - T_{sld}} L, T_{sld} \leq T < T_{lqd} \end{cases} \tag{17}$$

The selection of nanoparticles for enhancing PCM performance is based on several key criteria, which we have now elaborated on in this Section. These criteria include:

- Thermal conductivity: Nanoparticles with high thermal conductivity (e.g., Al2O3, CuO) are preferred to improve heat transfer within the PCM.
- Compatibility: The nanoparticles should be chemically inert and compatible with the PCM to avoid adverse reactions.
- Particle size and surface area: Smaller nanoparticles with high surface area-to-volume ratios are more effective in enhancing nucleation and heat transfer.
- Dispersion stability: Nanoparticles should be easily dispersible in the PCM to ensure uniform thermal properties.
- Cost and availability: Practical considerations such as cost and availability are also factored into the selection process.

The nanoparticles in Table 2 are considered the best for nanofluids due to their high thermal conductivity, stability, and unique properties that enhance heat transfer. The choice of nanoparticle depends on the specific application, cost considerations, and desired thermal performance. In summary the following nanoparticles used for investigation in this research whith the reasons provided:

1. Copper (Cu)

- High Thermal Conductivity: Cu has an exceptionally high thermal conductivity (~400 W/m·K), which significantly improves the heat transfer capability of the base fluid.

- Cost-Effective: Compared to noble metals like silver, Cu is relatively inexpensive, making it a practical choice for industrial applications.

- Wide Applications: Cu nanoparticles are widely used in cooling systems, heat exchangers, and electronic thermal management.

2. Silver (Ag)

- Exceptional Thermal Conductivity: Ag has the highest thermal conductivity among metals (~429 W/m·K), making it highly effective for enhancing heat transfer.

- Antimicrobial Properties: Ag nanoparticles also exhibit antimicrobial properties, which can be beneficial in biomedical and HVAC applications.

- Stability: Ag nanoparticles are relatively stable in fluids, though they are more expensive than Cu.

3. Copper Oxide (CuO)

- High Thermal Conductivity: CuO nanoparticles have a thermal conductivity of ~33 W/m·K, which is much higher than many base fluids.

- Cost-Effective and Stable: CuO is cheaper than metallic nanoparticles and exhibits good stability in nanofluids.

- Wide Temperature Range: CuO-based nanofluids are effective over a broad temperature range, making them suitable for high-temperature applications.

4. Aluminum Oxide (Al2O3)

- High Thermal Conductivity: Al2O3 nanoparticles have a thermal conductivity of ~30 W/m·K, which is significantly higher than water or ethylene glycol.

- Chemical Stability: Al2O3 is chemically inert and stable in most fluids, making it suitable for long-term use.

- Cost-Effective: Al2O3 is relatively inexpensive and widely available.

5. Titanium Dioxide (TiO2)

- Good Thermal Conductivity: TiO2 nanoparticles have a thermal conductivity of ~8.4 W/m·K, which is higher than many base fluids.

- Photocatalytic Properties: TiO2 nanoparticles are photocatalytic, making them useful in solar thermal applications and self-cleaning surfaces.

- Stability and Biocompatibility: TiO2 is stable in fluids and biocompatible, making it suitable

6. Single-Walled Carbon Nanotubes (SWCNT)

- Exceptional Thermal Conductivity: SWCNTs have an ultra-high thermal conductivity (~3,000–6,000 W/m·K), making them one of the best materials for enhancing heat transfer.

- High Aspect Ratio: Their high aspect ratio improves heat transfer pathways in the fluid.

- Lightweight and Strong: SWCNTs are lightweight and mechanically strong, making them ideal for advanced thermal management systems.

7. Multi-Walled Carbon Nanotubes (MWCNT)

- High Thermal Conductivity: MWCNTs have a thermal conductivity of ~3,000 W/m·K, similar to SWCNTs.

- Ease of Dispersion: MWCNTs are easier to disperse in fluids compared to SWCNTs due to their larger size.

- Cost-Effective: MWCNTs are cheaper than SWCNTs while still providing excellent thermal performance.

8. Graphene Nanoplatelets (GNP)

- Ultra-High Thermal Conductivity: GNPs have a thermal conductivity of ~5,000 W/m·K, making them one of the best materials for enhancing heat transfer.

- Large Surface Area: GNPs have a high surface area, which improves heat transfer at the nanoparticle-fluid interface.

- Lightweight and Flexible: GNPs are lightweight and flexible, making them suitable for advanced thermal management applications.

Table 2. Thermophysical properties.

	Specific Heat Capacity (J/kgK)	Density (kg m^3)	Thermal Conductivity (W m1K1)	Thermal Diffusivity ($\times 10^{-6} m^2 s^{-1}$)	Key Advantages
Cu	385	8933	400	116.3	High thermal conductivity, cost-effective
Ag	235	10500	429	173.9	Highest thermal conductivity, antimicrobial
CuO	540	6510	33	9.4	Stable, cost-effective, wide temperature range
Al2O3	765	3970	40	13.2	Chemically stable, cost-effective
TiO2	686.2	4250	8.954	3.1	Photocatalytic, biocompatible
SWCNT	425	2600	6600	5972.9	Ultra-high thermal conductivity, lightweight
MWCNT	796	1600	3000	2355.5	Easier dispersion, cost-effective
GNP	790	2200	5000	2876.9	Ultra-high thermal conductivity, large surface area
FR4 (Circuit Board)	1369	1900	0.3	0.115	-
Silica glass	703	2203	1.38	0.245	-
Solder (60Sn-40Pb)	150	9000	50	37.037	-

The PCM volume wall is FR4 without thermal resistance. The schematic of the problem is plotted in Figure 2. As shown the thermal resistance between the PCM enclosure and the surrounding air is considered negligible while the natural convection with coefficient of h = 10(W/m^{2}K is considered for heat transfer. Attaching a PCM heat sink requires some method that would incur resistance. The General configuration of the transistor is plotted in Figure 3. It is crucial to define thermophysical properties to analyze the change in NEPCM temperature during melting. As well the properties of the materials for thermal calculation are given in Table 2. Those properties are assumed to be independent of temperature. The PCM attached to the transistor, and it is the partially boundary condition of PCM at the back wall. The PCM enclosure consists of FR4.

The calculated properties of the NEPCMs are

Effective density:

$$\rho_{npcm} = \varphi\rho_p + (1-\varphi)\rho_{pcm}, \tag{18}$$

Effective specific heat capacity for NPs:

$$C_{p_{npcm}} = \frac{\varphi\rho_p C_{p_p} + (1-\varphi)\rho_{pcm} C_{p_{pcm}}}{\rho_{npcm}}, \tag{19}$$

Effective dynamic viscosity:

$$\mu_{npcm} = A_1 e^{(A_2 \cdot \varphi)} \mu_{pcm}, \tag{20}$$

Thermal conductivity:

$$k_{npcm} = \frac{k_p+2k_{pcm}-2(k_{pcm}-k_p)\varphi}{k_p+2k_{pcm}+(k_{pcm}-k_p)\varphi}k_{pcm} + 5.0x10^4\zeta\varphi\rho_{pcm}C_{p_{pcm}}\sqrt{\frac{B_oT}{\rho_p\phi_p}}[(2.82x10^{-2}\varphi + 3.92x10^{-3})\left(\frac{T}{T_r}\right) + (-3.07x10^{-2}\varphi - 3.91x10^{-3})], \quad (21)$$

where curve-fitting coefficients are shown in **Table 3.**

Table 3. Curve-fitting coefficients.

	A_1	A_2	ζ	C
Al_2O_3	0.983	12.96	$8.4(100\ \varphi)^{-1.07}$	0.425
CuO	0.920	22.85	$9.9(100\ \varphi)^{-0.95}$	-.—

2.4. Phase Dispersion, Separation and Thermal Aging

Dispersion of nanoparticles in PCM is indeed a critical challenge, as agglomeration can negatively impact thermal performance. Usually researchers employed the following methods:

- Surface functionalization: The nanoparticles (Al2O3, 50 nm in diameter) were surface-treated with oleic acid to improve their compatibility with TH29 and prevent agglomeration.
- Ultrasonic dispersion: The nanoparticles were dispersed in the PCM using a high-power ultrasonic homogenizer for 30 minutes to ensure uniform distribution.
- Stabilizers: A small amount of surfactant (0.1 wt%) was added to enhance long-term dispersion stability.

The nanoparticle concentration used in this study was 1.0 wt%, as this concentration was found to provide optimal thermal performance without significantly increasing viscosity or causing sedimentation.

The phase separation and thermal aging of phase change materials (PCMs) like TH29 are critical concerns for their long-term performance and reliability. Below is a detailed explanation of the limits of phase separation and thermal aging for TH29, supported by relevant references. Phase separation occurs when the components of a PCM (e.g., paraffin-based materials like TH29) separate into distinct phases due to repeated melting and solidification cycles. This can lead to inhomogeneity in the material, reducing its thermal storage capacity and heat transfer efficiency [31]. TH29, being an organic PCM, is prone to phase separation over prolonged thermal cycling. Studies have shown that paraffin-based PCMs can experience phase separation after 500–1,000 thermal cycles, depending on the purity of the material and the presence of additives or stabilizers. To address phase separation, nanoparticles (e.g., Al2O3, TiO2) or thickening agents are often added to improve the homogeneity and stability of the PCM. For example, it demonstrated that adding nanoparticles to paraffin-based PCMs significantly reduces phase separation and enhances thermal stability [32].

Thermal aging refers to the degradation of a PCM's thermophysical properties (e.g., latent heat, thermal conductivity) due to prolonged exposure to high temperatures and repeated thermal cycling. This can result in reduced cooling performance and shorter material lifespan. TH29, like other paraffin-based PCMs, typically exhibits a gradual reduction in latent heat capacity after 1,000–2,000 thermal cycles. The degradation rate depends on the operating temperature range and the presence of stabilizers. For instance, if TH29 is cycled repeatedly above its melting point (e.g., 50–60 °C), its thermal stability may degrade faster. Incorporating nanoparticles or microencapsulation techniques has been shown to improve the thermal stability of PCMs. researcher reported that nanoparticle-enhanced PCMs exhibit less than 5% degradation in latent heat after 1,000 cycles [33].

The combined effects of phase separation and thermal aging can significantly limit the performance of TH29 over time. Studies have shown that after 1,000 thermal cycles, paraffin-based PCMs like TH29 can experience up to 10–15% reduction in latent heat capacity and thermal conductivity due to phase separation and aging. The addition of nanoparticles or stabilizers can reduce this degradation to less than 5%, as demonstrated by Kibria et al. [34]. TH29 should ideally be used within its recommended temperature range (e.g., 20–60 °C) to minimize phase separation and thermal aging. Although here for a ransient condition more than usual range it used. Prolonged exposure to temperatures near or above its melting point can accelerate degradation. With proper stabilization

(e.g., nanoparticle addition), TH29 can maintain its performance for over 1,000 thermal cycles with minimal degradation. The phase separation and thermal aging limits of TH29 can be effectively managed through the addition of nanoparticles or stabilizers, which enhance its thermal stability and extend its lifespan. The references provided above offer detailed insights into the degradation mechanisms and mitigation strategies for paraffin-based PCMs like TH29.

3. Results

3.1. Electric Voltage and Heat Sources

Figure 4 presents the results of solving the voltage equation in the circuit. Based on the ground points at the transistor and the input electric currents at the three points shown in Figure 2. Heat source distributions are displayed in Figure 4. The electric current enters the transistor from the base and emitter and exits from the collector. Typical distribution voltages range from −10−4 to 10−4 V. Distribution circuits consist of electrical lines, as well as a transistor.

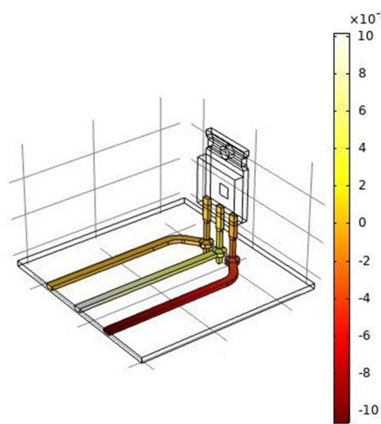

Figure 4. Results of voltage (V) distribution in the system.

The volumetric heat source distribution in the circuit and near connectors distribution in the device is shown in Figure 5. Based on the electric current and field the W near connectors is about 10 m^3 (about the volume of a storage unit). Once the local heat generation distribution is established, it can be used for calculating thermal distribution.

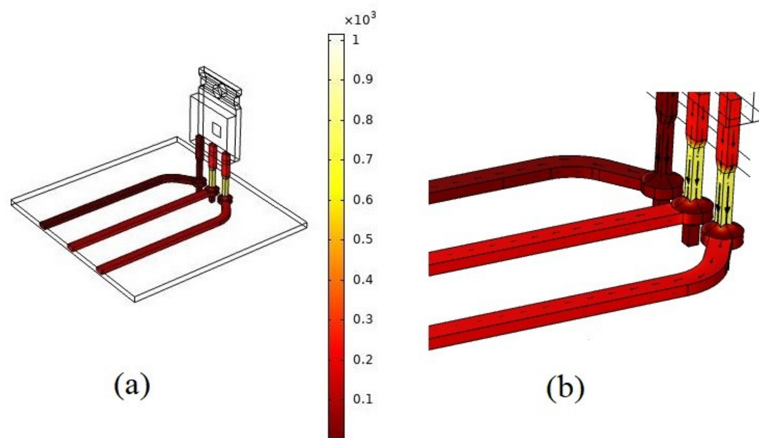

Figure 5. Heat generation variation within different region of electronic components (**a**) Volumetric heat source (W/m^3) distribution in the circuit; (**b**) Volumetric heat source distribution near connectors.

3.2. Temperature Distribution

General configuration with thermal iso surfaces is plotted in Figure 6. Approximately 80 degrees centigrade is the maximum temperature. A heat sink is not necessary since this temperature is within the operating range of the transistor. Also, it is important to recognize that electrical heating, or Joule heating, has negligible impact on the temperature of the copper routes far from the transistor. A significant amount of heat generated in the transistor chip is conducted away from the device through extremely conductive copper routes. General configuration of temperatures and thermal iso surfaces for Figure 6a compared with Transistor without PCM (see Figure 6b) and Transistor with PCM, (see Figure 6c) Transistor with NEPCM shows the temperature along the copper routes between the base and collector. Due to copper's high conductivity, the Joule heating effect does not increase the temperature in the copper routes since the current density in the base is 1/1000 that in the collector. Copper routes conduct heat away from this device. Circuit boards are thermally inefficient compared to copper routes. In the case without a PCM just conductive solid material same as FR4 properties is used the highest temperature is experienced while in NEPCM nanofluid containing solid PCM the minimum temperature rise is experienced. The nanofluid here is composed of the TH29 PCM with suspended Cu particles in.

As shown in Figure 6, the temperature exceeds 80 °C, it could lead to several issues, including:

Reduced transistor performance: Prolonged operation above the recommended temperature range can degrade the transistor's efficiency and lifespan.

Thermal runaway: Excessive heat can cause a positive feedback loop, further increasing temperatures and potentially leading to device failure.

Mechanical stress: Thermal expansion mismatches between materials can induce mechanical stresses, risking structural damage.

To mitigate these risks, our system incorporates the following safeguards:

Phase change material (PCM): The PCM absorbs excess heat during peak loads, preventing rapid temperature spikes.

Thermal management algorithm: The system includes a feedback-controlled cooling mechanism that adjusts the cooling rate based on real-time temperature monitoring.

Redundant cooling pathways: Additional heat dissipation pathways (e.g., heat sinks and fans) are activated if the temperature approaches critical levels.

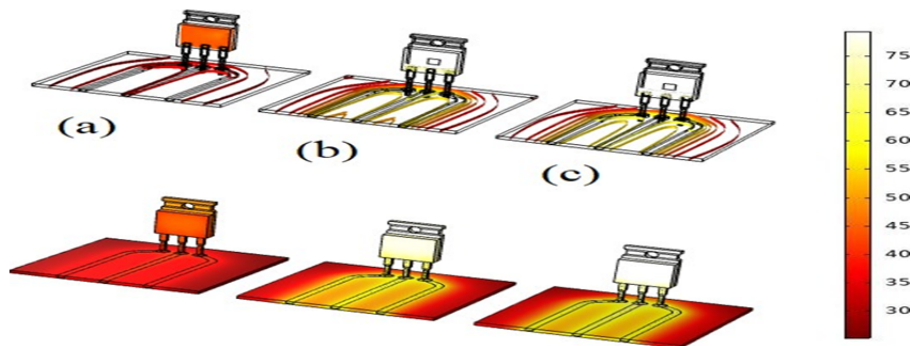

Figure 6. General configuration of temperatures and thermal iso surfaces for (**a**) Transistor without PCM; (**b**) Transistor with PCM; (**c**) Transistor with NEPCM.

Thermal iso surfaces in fluid PCM are plotted in Figure 7. In this figure, the liquid fraction contours at 10s for pure PCM are shown. NEPCMs containing carbon-based nanomaterials have an acceptable melting rate for the phase change process. Sometimes it is a little different from pure PCM. A liquid fraction contour plotted over time can be visualized in Figure 7. According to the picture, a higher temperature is near the transistor. The thermal conductivity of NEPCM affects the boundary layer formation. In buoyancy-driven convection currents shown here NEPCM accelerates the transfer of heat through conduction inside the boundary layer. The presence of NEPCM in fluid form at the upper part allows free convective heat transfer to become the primary mechanism for control volume. Melting rates increase dramatically in the PCM control volume due to the dominance of natural convection.

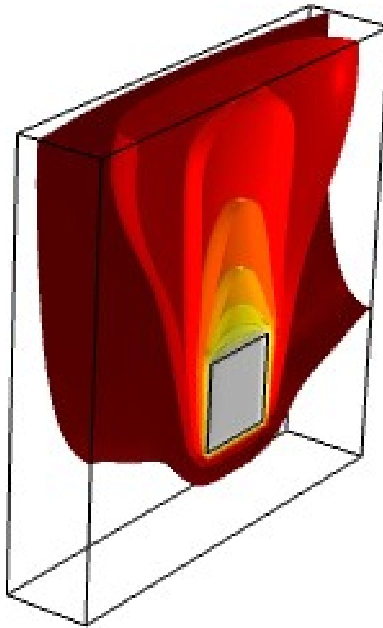

Figure 7. Thermal iso surfaces in fluid PCM.

The finite element method (FEM) code used to calculate heat and mass transfer is benchmarked by Jamalabadi and Park [1] as shown in Figure 8. As seen in Figure 8, they are in good agreement.

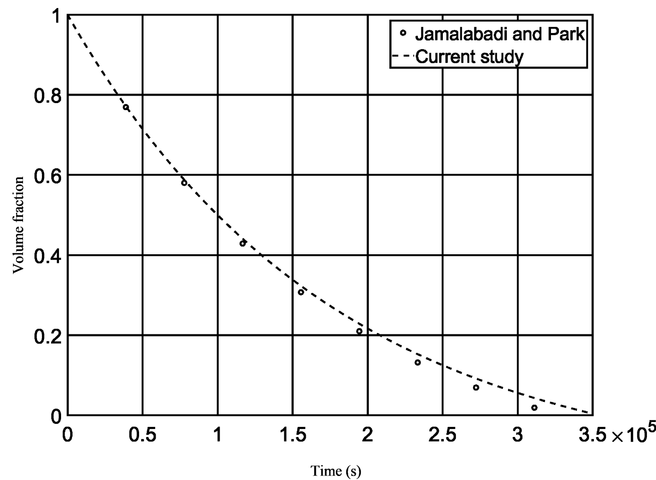

Figure 8. The of comparison the results of the current method with Jamaabadi and Park [1].

3.3. Phase Change

The phase change profile inside the NEPCM box is plotted in Figure 9. The charging time of NEPCM total melting time and liquid fraction are important parameters that pointed out here. Arrow plots of conductive heat flux and contour plots of pressure are presented in Figure 9 to illustrate how these parameters vary with nanomaterial concentration and nanomaterial type under the present model. Three types of nano additives are tested with concentrations of 1 percent. The liquid fraction contours of Figure 9 can increase by the concentration of NEPCMs, the conductive heat transfer is the reason. A fully melted PCM shows motion from left to right, and a solid PCM shows a blue color. There is a tiny mushy zone between them where the PCM is not able to move much. The density variation in the liquid PCM makes buoyancy-driven convection flows, and liquid at higher temperatures moves upward. PCM melts completely during this process.

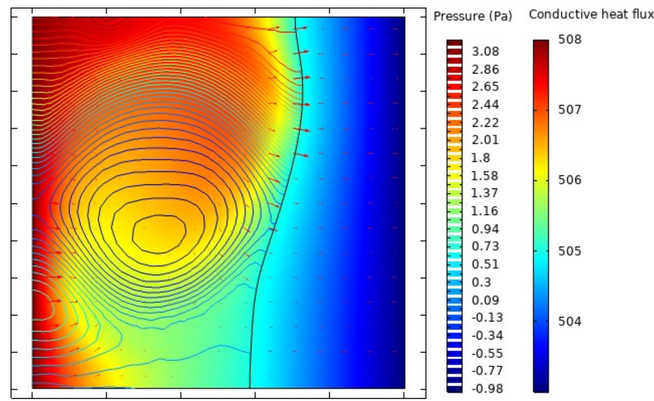

Figure 9. Phase change profile inside the NEPCM box.

General configuration with thermal volume contour is released in Figure 10. Figure 10a shows liquid volume fraction versus time for various nanoparticles. The time of process regarding conducted numerical experiments to evaluate the solid-liquid interface through various particles are MWCNT, GNP, SWCNT, Al2O3, TiO2, CuO, Cu, and Ag respectively. The time of finishing liquification and being a completely liquid in cavity. As well the temperature field on the transistor is shown and compared the maximum of the system. As well, curves in Figure 10a are too similar (the dark blues which can be distinguished) which shows the similarity of two results.

Figure 10b shows the maximum temperature on the transistor versus time. Through the various materials, the maximum to a minimum is SWCNT, GNP, MWCNT, Ag, Cu, Al2O3, CuO, and TiO2 respectively. Figure 10b does not have a control PCM compari- son because in a TH29 the temperature remains mostly near 29 degrees Celsius and then it is almost horizontal line. The discussion talks about improvements/reductions in performance which base line is near horizontal.

It is possible to positively influence the melting process of PCM by nanoparticles. Figure 10 illustrates this fact. Increasing the concentration of GNP, MWCNT, or SWCNT as shown in Figure 10 causes more liquid fractions. The carbon structure of this nanomaterial gives it higher performance, making it an ideal material for storing thermal energy. As shown in Table 2, carbon based nano materials have different thermophysical properties. Both cases have a similar transient liquid fraction. Due to higher conduction that nanomaterials provide, there is an enormous difference in it. Since graphene nanosheets have a plate structure, they have a superior thermal conductivity to carbon nanotubes. It is evident that graphene nanosheets have an admirable superiority over carbon nanotubes. Conduction of the material is increased by GNP into it, while SWCNT-PCM and MWCNT-PCM display increased conductivity less.

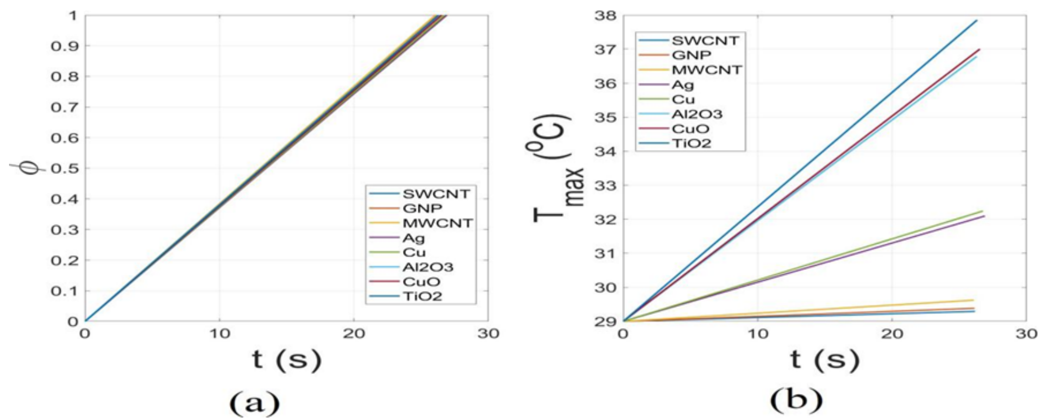

Figure 10. General configuration of using various nano particles (**a**) liquid volume fraction versus time; (**b**) Maximum temperature on transistor versus time.

Temperature distribution vs distance from the connector for various cooling scenarios are depicted in Figure

11. For NEPCMs with different nano additives, Figure 11 illustrates the temperature changes over electric conductive materials. The temperature rise caused by electric heat loss is shorter when carbon-based nanomaterials are applied to surfaces with high thermal conductivity. NEPCMs do not differ significantly from each other. Although temperatures between the different NEPCMs are huge but the temperature changes within the electric conductor because of changes at PCM control volume.

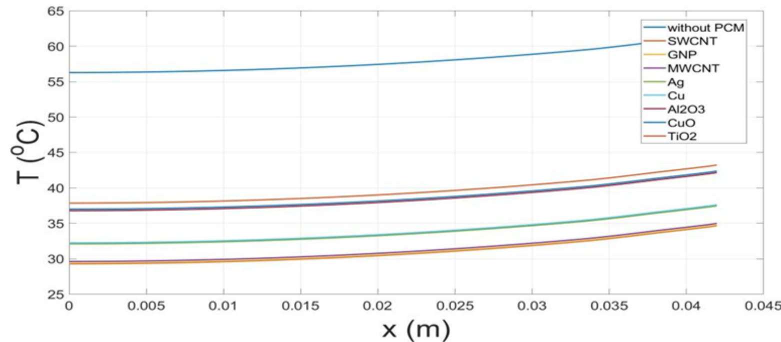

Figure 11. Temperature distribution vs distance from the connector for various cooling scenarios.

4. Discussion

The first section examines temperature distributions in the solid part examined by the electric analysis. Results are broken down into several sections. Then the transient liquid fraction's effects on nano-additives are examined. Using streamlines and liquidity ratio contours are good explained through control volume. Afterward, the study focused on transient temperature contours and temperature distributions of NEPCM containing various nano-additives. In the end, PCM with the influence of nanomaterials is explored. The comparison give the ability to better understand how nano-additives affect melting.

Figure 9 shows nanoadditives' effects on transient liquid fractions based on their concentrations. Metal based particles reduce the ratio of liquid volume when their concentration is increased. For metal oxide nanomaterials, indicating that the liquid fraction grows very slowly as Al2O3 nanoparticle concentrations increase (see Figure 9a). Nanoparticles such as TiO2 and CuO, however, behave oppositely. Considering nanomaterials' thermophysical properties can explain this difference. Even though metal based nanofluids, improved conduction, they exhibit very poor melting properties due to their high density and low specific heat. Thus, if the added values of viscosity and density are not outweighed by improving the NEPCM thermal conduction, then the melting process will be unreliable. There are almost no significant differences in PCM melting characteristics when CuO and TiO2 are used as a nanoparticle in NEPCM even for various concentrations (lowest slope lines in figures).

In Figure 11 the PCM control line could be considered as 29 degrees' Celsius horizontal for comparison. Without PCM, higher temperatures reach in a sooner time scales. Colors in Figure 11 are attributed to various NEPCM. As shown, the SWCNT sample is the best while the sample has better temperatures, and the melting rate does not appear to be significantly different. The plain PCM case claims that nanoparticle additives show increased performance. The results could be expanded upon to include more information on the melting progression and impact of natural convection that changes with different nanoparticle chemistries.

5. Conclusions

Enhanced thermophysical characteristics of NEPCMs at different concentrations on the cooling of the power transistor were examined. These nano particles included metal nanoparticles (Cu and Ag), metal oxide nanoparticles (Al2O3, CuO, TiO2), and carbon nanoparticles (GNP, MWCNT, SWCNT). The phase changes final time, crucial for the design of PCM storage, is obtained. Using NePCM simulations were conducted to predict the thermal characteristics of a PCM control volume system. The conclusion of the current study is:

- The best performance is shown by NEPCMs containing GNP.
- The melting time increases compared to pure PCM.
- There is a slight improvement in maximum temperature SWCNT-PCM and MWCNT PCM.

- As compared to pure PCM, TiO2-PCM is quite similar in performance.
- PCM melts faster when nanoparticles are added.
- The time of process regarding conducted numerical experiments to evaluate the solid-liquid interface through various particles are MWCNT, GNP, SWCNT, Al2O3, TiO2, CuO, Cu, and Ag respectively.
- Through the various materials, the maximum temperature on the transistor surface is obtained by SWCNT, GNP, MWCNT, Ag, Cu, Al2O3, CuO, and TiO2 respectively.

The results could be expanded upon to include more information on the melting progression and impact of natural convection that changes with different nanoparticle chemistries.

Funding

This work received no external funding.

Institutional Review Board Statement

Not applicable.

Informed Consent Statement

Not applicable.

Data Availability Statement

The data supporting the finding of this study are available upon reasonable request.

Conflicts of Interest

The authors declare no conflict of interest.

References

1. Abdollahzadeh Jamalabadi, M.Y.; Park, J.H. Effects of Brownian motion on freezing of PCM containing nanoparticles. *Therm. Sci.* **2016**, *20*, 1533–1541.
2. Abdollahzadeh Jamalabadi, M.Y.; Park, J.H. Investigation of Property Variations on Freezing of PCM containing Nanoparticles. *World Appl. Sci. J.* **2014**, *32*, 672–677.
3. Abdollahzadeh Jamalabadi, M.Y. Feasibility Study of Cooling a Bulk Acoustic Wave Resonator by Nanoparticle Enhanced Phase Change Material. *Magnetochemistry* **2021**, *7*, 0.
4. Abdollahzadeh Jamalabadi, M.Y. Magnetohydrodynamic and Nanoparticle Effects in Vertical Annular Subcooled Flow Boiling. *Symmetry* **2019**, *11*, 810.
5. Abdollahzadeh Jamalabadi, M.Y. Use of Nanoparticle Enhanced Phase Change Material for Cooling of Surface Acoustic Wave Sensor. *Fluids* **2021**, *6*, 31.
6. Ali, H.M. Recent advancements in PV cooling and efficiency enhancement integrating phase change materials based systems–A comprehensive review. *Sol. Energy* **2020**, *197*, 163–198.
7. Hassan, A.; Wahab, A.; Qasim, M.A.; et al. Thermal management and uniform temperature regulation of photovoltaic modules using hybrid phase change materials-nanofluids system. *Renewable Energy* **2020**, *14*, 282–293.
8. Tuckerman, D.B.; Pease, R.F.W. High-performance heat sinking for VLSI. *IEEE Electron Device Lett.* **1981**, *2*, 126–129.
9. Ho, C.J.; Huang, C.S.; Qin, C.; et al. Thermal performance of phase change nano-emulsion in a rectangular minichannel with wall conduction effect. *Int. Commun. Heat Mass Transfer* **2020**, *110*, 104438.
10. Alehosseini, E.; Jafari, S.M. Micro/nano-encapsulated phase change materials (PCMs) as emerging materials for the food industry. *Trends Food Sci. Technol.* **2019**, *91*, 116–128.
11. Hajjar, A.; Mehryan, S.; Ghalambaz, M. Time periodic natural convection heat transfer in a nano-encapsulated phase-change suspension. *Int. J. Mech. Sci.* **2020**, *166*, 105243.
12. Davidson, J.L.; Bradshaw, D.T. Compositions with nano-particle size conductive material powder and meth-

ods of using same for transferring heat between a heat source and a heat sink. United States Patent. US7390428B2, 2008.
13. Sardarabadi, M.; Passandideh-Fard, M.; Maghrebi, M.J.; et al. Experimental study of using both ZnO/water nanofluid and phase change material (PCM) in photovoltaic thermal systems. *Sol. Energy Mater. Sol. Cells* **2017**, *161*, 62–69.
14. Bahiraei, M.; Jamshidmofid, M.; Goodarzi, M. Efficacy of a hybrid nanofluid in a new microchannel heat sink equipped with both secondary channels and ribs. *J. Mol. Liq.* **2019**, *273*, 88–98.
15. Martínez, V.A.; Vasco, D.A.; García-Herrera, C.M.; et al. Numerical study of TiO2-based nanofluids flow in microchannel heat sinks: Effect of the Reynolds number and the microchannel height. *Appl. Therm. Eng.* **2019**, *161*, 114130.
16. Zografos, A.I.; Martin, W.A.; Sunderland, J.E. Equations of properties as a function of temperature for seven fluids. *Comput. Methods Appl. Mech. Eng.* **1987**, *61*, 177–187.
17. Ding, M.; Liu, C.; Rao, Z. Experimental investigation on heat transfer characteristic of TiO2-H2O nanofluid in microchannel for thermal energy storage. *Appl. Therm. Eng.* **2019**, *160*, 114024.
18. Ho, C.J.; Liu, Y.C.; Ghalambaz, M.; et al. Forced convection heat transfer of nano-encapsulated phase change material (NEPCM) suspension in a mini-channel heatsink. *Int. J. Heat Mass Transfer* **2020**, *155*, 119858.
19. Ho, C.J.; Chang, P.; Yan, W.; et al. Thermal and Hydrodynamic Characteristics of Divergent Rectangular Minichannel Heat Sinks. *Int. J. Heat Mass Transfer* **2018**, *122*, 264–274.
20. Chabi, A.R.; Zarrinabadi, S.; Peyghambarzadeh, S.M.; et al. Local convective heat transfer coefficient and friction factor of CuO/water nanofluid in a microchannel heat sink. *Heat Mass Transfer* **2017**, *53*, 661–671.
21. Ho, C.J.; Liao, J.C.; Li, C.H.; et al. Experimental study of cooling performance of water-based alumina nanofluid in a minichannel heat sink with MEPCM layer embedded in its ceiling. *Int. Commun. Heat Mass Transfer* **2019**, *103*, 1–6.
22. Kumar, V.; Sarkar, J. Particle ratio optimization of Al2O3-MWCNT hybrid nanofluid in minichannel heat sink for best hydrothermal performance. *Appl. Therm. Eng.* **2020**, *165*, 114546.
23. Gupta, M.; Singh, V.; Kumar, R.; et al. A review on thermophysical properties of nanofluids and heat transfer applications. *Renewable Sustainable Energy Rev.* **2017**, *74*, 638–670.
24. Rai, A.K.; Kumar, A. A review on phase change materials and their applications. *Int. J. Adv. Res. Eng. Technol.* **2012**, *3*, 214–225.
25. Zhao, C.Y.; Zhang, G.H. Review on microencapsulated phase change materials (MEPCMs): fabrication, characterization and applications. *Renewable Sustainable Energy Rev.* **2011**, *15*, 3813–3832.
26. Liu, C.; Rao, Z.; Zhao, J.; et al. Review on nanoencapsulated phase change materials: preparation, characterization and heat transfer enhancement. *Nano Energy* **2015**, *13*, 814–826.
27. Ho, C.J.; Chen, W.C.; Yan, W.M. Experimental study on cooling performance of minichannel heat sink using water-based MEPCM particles. *Int. Commun. Heat Mass Transfer* **2013**, *48*, 67–72.
28. Ho, C.J.; Chen, W.C.; Yan, W.M. Correlations of heat transfer effectiveness in a minichannel heat sink with water-based suspensions of Al2O3 nanoparticles and/or MEPCM particles. *Int. J. Heat Mass Transfer* **2014**, *69*, 293–299.
29. Muthya Goud, V.; Vaisakh, V.; Joseph, M.; et al. An experimental investigation on the evaporation of polystyrene encapsulated phase change composite material based nanofluids. *Appl. Therm. Eng.* **2020**, *168*, 114862.
30. Okonkwo, E.C.; Wole-Osho, I.; Almanassra, I.W.; et al. An updated review of nanofluids in various heat transfer devices. *J. Therm. Anal. Calorim.* **2021**, *145*, 2817–2872.
31. Zamani, J.; Keshavarz, A. Genetic algorithm optimization for double pipe heat exchanger PCM storage system during charging and discharging processes. *Int. Commun. Heat Mass Transfer* **2023**, *146*, 106904. [CrossRef]
32. Kibria, M.; Anisur, M.; Mahfuz, M.; et al. A review on thermophysical properties of nanoparticle dispersed phase change materials. *Energy Convers. Manage.* **2015**, *95*, 69–89. [CrossRef]
33. Tchanche, B.F.; Pétrissans, M.; Papadakis, G. Heat resources and organic Rankine cycle machines. *Renewable Sustainable Energy Rev.* **2014**, *39*, 1185–1199. [CrossRef]
34. Zhang, P.; Xiao, X.; Ma, Z. A review of the composite phase change materials: Fabrication, characterization, mathematical modeling and application to performance enhancement. *Appl. Energy* **2016**, *165*, 472–510.

Copyright © 2024 by the author(s). Published by UK Scientific Publishing Limited. This is an open access article under the Creative Commons Attribution (CC BY) license (https://creativecommons.org/licenses/by/4.0/).

Publisher's Note: The views, opinions, and information presented in all publications are the sole responsibility of the respective authors and contributors, and do not necessarily reflect the views of UK Scientific Publishing Limited and/or its editors. UK Scientific Publishing Limited and/or its editors hereby disclaim any liability for any harm or damage to individuals or property arising from the implementation of ideas, methods, instructions, or products mentioned in the content.